Available online at www.sciencedirect.com
SCIENCE DIRECT®
Journal of Sound and Vibration 262 (2003) 769–793
JOURNAL OF SOUND AND VIBRATION
www.elsevier.com/locate/jsvi

Rotor vibration reduction with polymeric sectors

J.K. Dutt[a,*], T. Toi[b]

[a] Department of Mechanical Engineering IIT, Kharagpur 721302, West Bengal, India
[b] Department of Precision Mechanics, Chuo University, 1-13-27 Kasuga Bunkyo-ku, Tokyo 112-8551, Japan

Received 20 June 2001; accepted 20 June 2002

Abstract

This work has been undertaken principally with an idea to improving the dynamic performance of rotor–shaft systems, which often suffer from two major problems (a) resonance and (b) loss of stability, resulting in excessive vibration of such systems. Polymeric material in the form of sectors has been considered in this work as bearing supports. Polymeric material has been considered in this work as both stiffness and loss factor of such materials varies with the frequency of excitation. Stiffness and loss factor have been found out for the proposed support system comprising of polymeric sectors. Depending upon the frequency of excitation the system matrix, in this case, changes and dynamic performance of the rotor–shaft system also changes accordingly. Here in this work avoidance of resonance and application of optimum damping in the support have been investigated by finding out the optimum dimension, i.e., the optimum thickness and optimum length of the sectors. It has been theoretically found that use of such sectors reduces the rotor unbalanced response, increases the stability limit speed for simple rotor–shaft systems and thus improves the dynamic characteristics. Parameters of the system have been presented in terms of non-dimensional quantities. Many examples have been presented in support of the conclusion. The life of such supports, particularly in the presence of chemicals and other reagents has not been investigated.

1. Introduction

Rotating machinery primarily comprise of shaft, discs representing gears or blades depending upon the use and bearings to support the load as well as to help in rotation. Rotary power is fed to the rotor from motor or any prime mover for rotation. Ideally, the rotor should only execute rotation but due to several excitations either external or internal by nature, rotating machinery suffer generally from two operational difficulties from dynamic point of view. These difficulties

*Corresponding author. Tel.: +91-3222-777961; fax: +91-3222-755303.
E-mail address: jkdutt@camal.mech.chuo-u.ac.jp (J.K. Dutt).

0022-460X/03/$ - see front matter
doi:10.1016/S0022-460X(02)01081-7

are (a) high amplitude of vibration due to resonance and (b) self-excited vibration of the system also termed as the loss of stability. Important causes for external excitations are unbalance in the rotor or in the shaft, misalignment in the coupling, lack of straightness of the shaft out of many others. Internal excitation or self-excitation is caused when the characteristic of the system becomes such that the rotary power magnifies and supports any little perturbation to the system. Both these forms of excitations and the resulting outcome are unwanted from the points of view of operational ease, integrity safety and reliability. Hence, many attempts have been taken so far to reduce these effects and are reported in the literature. By and large all these attempts were to provide damping at the support as this has been observed to cure the above difficulties by dissipating the unwanted vibratory energy. Refs. [1,2] out of many others reported the improvement of overall dynamic characteristics calculated in terms of synchronous response amplitude of the rotor due to unbalance and the stability limit speed of the rotor–shaft system when supports were added. Existence of support properties corresponding to optimum dynamic performance was also reported. Out of many works on predicting the optimum support properties an interesting one is by Pilkey et al. [3], where the authors used the "linear programming technique" to predict the optimum support characteristics. Damping is a mechanism to dissipate mechanical energy in the form of heat. The quest for more efficient energy dissipating mechanism showed that the polymeric materials were very useful. Mallik [4] reported many uses of the polymeric supports. The handbook written by Darlow and Zorzi [5] reported many uses of these materials for reducing the amplitude of rotor vibration. Zorzi's experiments reported in Ref. [6] further consolidated the use of polymeric elements as useful support material as it showed the efficiency of polymeric support materials over the squeeze film dampers in reducing vibration amplitude. Polymer science is a rapidly emerging area of technical excellence. A detailed record by Corsaro and Sperling [7] shows that the chemists are now able to synthesize polymers with desired mechanical properties. Inspired by the recent developments, Dutt and Nakra [8,9] predicted the polymeric characteristics that can improve the dynamic characteristics of simple rotor–shaft systems. The work presented in Ref. [9], is an example to show that frequency-dependent stiffness and loss factor of the polymeric supports can be predicted in such a way that resonance can be avoided by suitably changing the natural frequencies of a simple rotor–shaft system. Recently, Panda and Dutt [10] reported an optimization technique to predict optimum feasible support characteristics to minimize the unbalanced response (UBR) and maximize the stability limit speed (SLS). The Ph.D. dissertation of Dutt [11] may be seen for details of calculations of UBR and SLS of rotor–shaft system on polymeric supports. In all the references cited above the authors concentrated more on the characteristics of the supports but did not report the true geometrical design of such supports, the relationship, the support properties bear with the dimension, and the placement of supports. These were truly attempted here.

2. Analysis

2.1. Properties of a polymeric element

The elastic modulus E and the modulus of rigidity G represent the properties of any material. These are independent of the dimension of any material. In the case of polymers also the same is

true. The only difference is that unlike metals, where E and G are constants, these are functions of operators of time in the case of polymers. Therefore, the value of E or G is dependent on the nature of loading for polymers. Let us take the example of a polymeric bar of length l, width w and thickness t as shown in Fig. 1(a). Load displacement characteristics of polymeric elements can be represented using multi-element spring damper model. Figs. 1(b) and (c) show the 3- and 4-element models respectively. For the 3-element model "K_1" may be called the primary support stiffness, K_2, the secondary support stiffness and C_1, the support damping coefficient. Other more complicated multi-element models can also be used. Force displacement relationships obtained by using 3- and 4-element models are given below. Detailed process for finding the relationships can be found in Bland [12]. Here in this work the 3-element model has been used, firstly due to its simplicity and secondly for getting an easy insight into the effect that each support parameter has on the dynamic response of the rotor–shaft system.

$$F = K(\,)\delta. \tag{1}$$

In the above expression F is the force, $K(\,)$, represents the stiffness operator and δ is the displacement.

For the 3-element model

$$K(\,) = \frac{\gamma_1 + \gamma_2 D}{1 + \alpha_1 D}, \tag{2}$$

where $\gamma_1 = K_1,\ \gamma_2 = K_1 C_1/K_2 + C_1,\ \alpha_1 = C_1/K_2$.

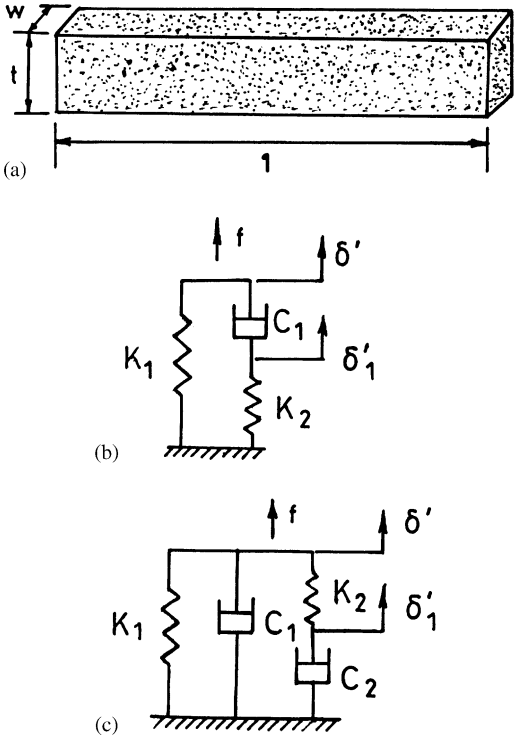

Fig. 1. (a) The polymeric bar; (b) 3-element model and (c) 4-element model.

For the 4-element model

$$K(\,) = \frac{\gamma_1 + \gamma_2 D + \gamma_3 D^2}{1 + \alpha_1 D}, \tag{3}$$

where $\gamma_1 = K_1$, $\gamma_2 = C_1 + C_2 + K_1 C_2/K_2$, $\gamma_3 = C_1 C_2/K_2$.

The symbol "D" represents $\mathrm{d}/\mathrm{d}t$. Using the expression of the stiffness operator, the expression of the elastic modulus can be obtained as given below in Eq. (4).

$$E(\,) = \frac{l}{wt} K(\,) \tag{4}$$

Relationship between E and G for polymers is given by

$$G(\,) = \frac{E(\,)}{2(1+\mu)} \tag{5}$$

In Eq. (4) μ is the Poisson's ratio. The value of μ is close to 0.5 for rubber like materials. For metals this is a constant but in the case of polymers this varies depending upon conditions of loading displacement and may be upon composition.

2.2. The support system

Fig. 2(a) shows the support system. Polymeric sectors, *each of same material*, are inserted in the annular space between the outer race of the bearing and the bearing housing and are considered glued on both the housing and the inner race. It has been assumed that the force of compression together with the effect of gluing is sufficient to prevent the outer race from rotating. Any general movement of the outer race of the bearing loads the sector with a dual effect of compression and shear. The net effect may, depending upon the location of the sector, increase or decrease the initial compressive force. Fig. 2(b) shows the effect of a vertical movement of the outer race.

2.2.1. Stiffness operator of the general support system

Fig. 3 shows the support system with many polymeric inserts. Suppose that the number of sectors is "n". Radius of the outer race is r and the thickness of the polymeric sector is t. Material of all the inserts is assumed to be same. The principle of linear viscoelastic solid has been considered for modeling the sectors. We consider here the ith sector, i.e., the sector between the angles θ_{1i} and θ_{2i}. Fig. 4 shows this sector. We suppose that the outer race has a movement of δ_x along the X direction and δ_y along the Y direction. Considering an infinitesimal trapezoidal polymeric element shown cross-hatched, of length δ_φ at an angular location φ, the displacements along radial and cross-radial directions, i.e., along r and φ directions will, respectively, be

$$\delta_r = \delta_x \cos\varphi + \delta_y \sin\varphi, \tag{6}$$

$$\delta_\varphi = -\delta_x \sin\varphi + \delta_y \cos\varphi. \tag{7}$$

The deformation δ_r being in the radial direction will cause compression and δ_φ being along the cross-radial direction will cause shear. It may be noticed from the expressions that the

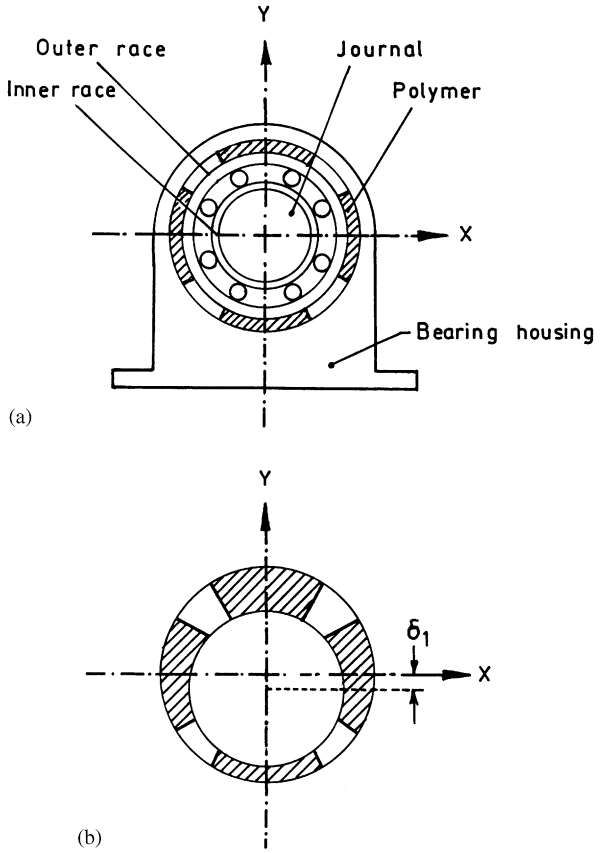

Fig. 2. (a) The support system; and (b) Movement of the outer race by δ.

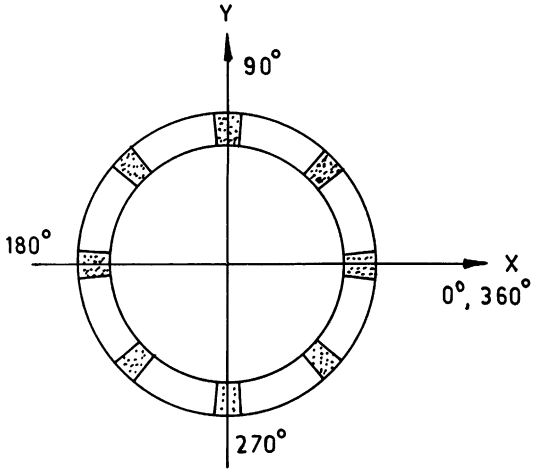

Fig. 3. The support system with eight symmetric sectors.

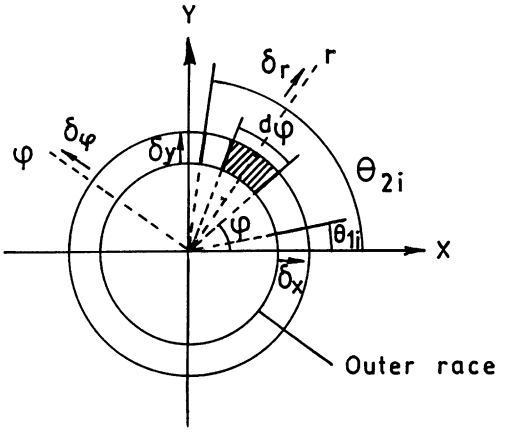

Fig. 4. Displacement of polymeric element under combined loads.

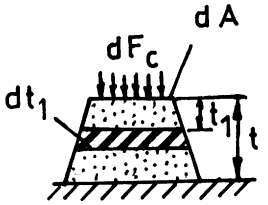

Fig. 5. The element in compression.

deformations vary as the location of the section varies. Let us consider the thin slice subjected to these deformations. Fig. 5 shows the enlarged infinitesimal element. Area of the face of a strip, of thickness dt_1, at a depth t_1 from the top is given by $\big((r+t_1)/r\big)\,dA$, where $dA=(rw)\,d\varphi$ is the area of the top surface. Total deflection under the influence of a compressive force $d(F_c)$ is given by

$$\Delta_c=\int_0\frac{d(F_c)*dt_1}{\big((r+t_1)/r\big)(rw)E(\,)\,d\varphi}=\frac{d(F_c)r}{(rw)\,d\varphi E(\,)}\ln\left|\frac{r+t}{r}\right|. \tag{8}$$

In the above expression the subscript "c" indicates the case for compressive deformation.

The infinitesimal force can be expressed as

$$d(F_c)=\frac{wE(\,)\Delta_c(d\varphi)}{\ln\left|\dfrac{r+t}{r}\right|}. \tag{9}$$

Writing $\Delta_c=\delta_r=\delta_x\cos\varphi+\delta_y\sin\varphi$, we get

$$d(F_c)=\frac{wE(\,)(\delta_x\cos\varphi+\delta_y\sin\varphi)(d\varphi)}{\ln\left|(r+t)/r\right|}. \tag{10}$$

The cosine component of this force works along the X direction and the sine component works in the Y direction. Writing the infinitesimal forces along X and Y directions as $\mathrm{d}(F_{cxi})$ and $\mathrm{d}(F_{cyi})$, respectively, and integrating from $\varphi = \theta_{1i}$ to $\varphi = \theta_{2i}$ the expressions of the forces due to compression, F_{cxi} acting in the X direction and F_{cyi} acting in the Y direction are obtained as given in Eqs. (11) and (12):

$$F_{cxi} = \int_{\theta_{1i}}^{\theta_{2i}} \mathrm{d}F_{cxi} = \frac{wE(\,)}{\ln|(r+t)/r|}\left[\delta_x\left\{\frac{\theta_{2i}-\theta_{1i}}{2}+\frac{\sin 2\theta_{2i}-\sin 2\theta_{1i}}{4}\right\}+\delta_y\left(\frac{\cos 2\theta_{1i}-\cos 2\theta_{2i}}{4}\right)\right], \tag{11}$$

$$F_{cxi} = \int_{\theta_{1i}}^{\theta_{2i}} \mathrm{d}F_{cyi} = \frac{wE(\,)}{\ln|(r+t)/r|}\left[\delta_x\left(\frac{\cos 2\theta_{1i}-\cos 2\theta_{2i}}{4}\right)+\delta_y\left\{\frac{\theta_{2i}-\theta_{1i}}{2}-\frac{\sin 2\theta_{2i}-\sin 2\theta_{1i}}{4}\right\}\right]. \tag{12}$$

Considering the same element in Fig. 5, shown again in Fig. 6, where it is subjected to shear deformation $\Delta_s = \delta_\varphi = -\delta_x \sin\varphi + \delta_y \cos\varphi$, (subscript s for shear deformation), and following the same procedure as in the case of finding the compressive deformation, infinitesimal force for shear deformation "$\mathrm{d}F_s$" is obtained and given below in Eq. (13):

$$\mathrm{d}(F_s) = \frac{wG(\,)\Delta s(\mathrm{d}\varphi)}{\ln|(r+t)/r|}. \tag{13}$$

The cosine component of this force acts in the Y direction and the sine component acts in the *negative* X direction. Integrating all the infinitesimal forces along X and Y directions the expressions of net shear deformation force due to the ith element "F_{sxi}" and "F_{syi}" are obtained as given in Eqs. (14) and (15):

$$F_{sxi} = \int_{\theta_{1i}}^{\theta_{2i}} \mathrm{d}F_{sxi} = \frac{wG(\,)}{\ln|(r+t)/r|}\left[\delta_x\left\{\frac{\theta_{2i}-\theta_{1i}}{2}-\frac{\sin 2\theta_{2i}-\sin 2\theta_{1i}}{4}\right\}-\delta_y\left(\frac{\cos 2\theta_{1i}-\cos 2\theta_{2i}}{4}\right)\right]. \tag{14}$$

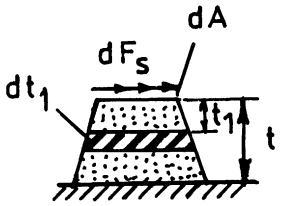

Fig. 6. The element in shear.

$$F_{syi} = \int_{\theta_{1i}}^{\theta_{2i}} \mathrm{d}F_{syi} = \frac{wG(\,)}{\ln|(r+t)/r|}\left[\delta_x\left(\frac{\cos 2\theta_{2i} - \cos 2\theta_{1i}}{4}\right) + \delta_y\left\{\frac{\theta_{2i} - \theta_{1i}}{2} + \frac{\sin 2\theta_{2i} - \sin 2\theta_{1i}}{4}\right\}\right]. \quad (15)$$

Expressions of total forces "F_x^i" and "F_y^i" acting along X and Y directions can be obtained by adding the expressions given by Eqs. (11) and (14) and those given by the Eqs. (12) and (15), respectively. Using the expressions of $E(\,)$ and $G(\,)$ given in Eqs. (4) and (5), the expression of length of the polymeric sector $l = (r + 0.5t)*(\theta_{2i} - \theta_{1i})$ and putting the non-dimensional term $\mu_p = t/r$ expressions of F_x^i and F_y^i are obtained as given in Eqs. (16) and (17):

$$F_x^i = F_{cxi} + F_{sxi} = k_{xx}^i(\,)\delta_x + k_{xy}^i(\,)\delta_y, \quad (16)$$

$$F_y^i = F_{cyi} + F_{syi} = k_{yx}^i(\,)\delta_x + k_{yy}^i(\,)\delta_y, \quad (17)$$

where

$$k_{xx}^i(\,) = k_1^i K(\,), \quad k_{xy}^i(\,) = k_{yx}^i(\,) = k_2^i K(\,) \quad \text{and} \quad k_{yy}^i(\,) = k_3^i K(\,), \quad (18)$$

$$k_1^i = \frac{(2+\mu_p)(\theta_{2i} - \theta_{1i})}{16(1+\mu)\mu_p \ln(1+\mu_p)}[(6+4\mu)(\theta_{2i} - \theta_{1i}) + (1+2\mu)(\sin 2\theta_{2i} - \sin 2\theta_{1i})], \quad (19)$$

$$k_2^i = \frac{(2+\mu_p)(\theta_{2i} - \theta_{1i})}{16(1+\mu)\mu_p \ln(1+\mu_p)}[(1+2\mu)(\cos 2\theta_{1i} - \cos 2\theta_{2i})], \quad (20)$$

$$k_3^i = \frac{(2+\mu_p)(\theta_{2i} - \theta_{1i})}{16(1+\mu)\mu_p \ln(1+\mu_p)}[(6+4\mu)(\theta_{2i} - \theta_{1i}) - (1+2\mu)(\sin 2\theta_{2i} - \sin 2\theta_{1i})], \quad (21)$$

where k_1^i, k_2^i, k_3^i are dimensionless constants for the ith polymeric sector.

Summing all the forces along X and Y directions for all the sectors the expressions of F_x and F_y are obtained as given in Eqs. (22) and (23):

$$F_x = \sum_1^n F_x^i = \sum_1^n k_{xx}^i(\,)\delta_x + \sum_1^n k_{xy}^i(\,)\delta_y = K_1^c K(\,)\delta_x + K_2^c K(\,)\delta_y, \quad (22)$$

$$F_y = \sum_1^n F_y^i = \sum_1^n k_{yx}^i(\,)\delta_y + \sum_1^n k_{yy}^i(\,)\delta_y = K_2^c K(\,)\delta_x + K_3^c K(\,)\delta_y, \quad (23)$$

$$K_1^c = \sum_1^n k_1^i, \quad K_2^c = \sum_1^n k_2^i, \quad K_3^c = \sum_1^n k_3^i.$$

Value of the constants K_1^c, K_2^c and K_3^c depends upon the geometry and placement and not upon the material of the sectors. From Eqs. (16) and (17) as well as from Eqs. (22) and (23) it may be seen that, in general, the forces are coupled, i.e., a displacement in the X direction generates a force in the Y direction and vice versa. When subjected to sinusoidal excitation causing sinusoidal displacement functions, the stiffness operators give rise to complex expressions of the stiffness where the real part is the stiffness, in-phase with the force, and the imaginary part is due stiffness in-quadrature with the force. Considering the stiffness operator given in Eq. (2) for the 3-element model to operate on a sinusoidal displacement function of frequency ω, it is possible to express the stiffness in the complex form

$$K_{real}(1 + i\eta). \tag{24}$$

In Eq. (24) K_{real}, the in-phase stiffness and η, the loss factor are given as

$$K_{real} = \left(\frac{\gamma_1 + \omega^2\alpha_1\gamma_2}{1 + \omega^2\alpha_1^2}\right), \quad \eta = \left(\frac{\omega\gamma_2 - \omega\alpha_1\gamma_1}{\gamma_1 + \omega^2\alpha_1\gamma_2}\right). \tag{25}$$

Expressions of K_{real} and η change with the model that represents the support.

2.3. Unbalanced response

2.3.1. Assumptions

Fig. 7 shows the schematic diagram of the rotor–shaft system. The rotor of mass M_2 is placed in the middle of the mass less rotor–shaft with stiffness K_s at the location of the disc and having viscous internal damping the coefficient of which is "c_i". The shaft is mounted on identical bearings of stiffness $K_b/2$ each and negligible damping coefficient. It is considered that the restoring force due to the bearing varies linearly with the deformation of the bearing elements. Rolling element bearings have been considered in this work. Though in reality rolling element bearings offer restoring force varying nonlinearly with deformation of the elements, yet, the effect of non-linearity in such cases is not much pronounced particularly in the presence of external damping due to the polymeric damping materials in this case. Refs. [11,13] may be seen for the effect of non-linear restoring force. Bearings on both sides are supported on identical supports, i.e., the number, material and position of polymer sectors on two sides are identical. Total mass of the bearings is M_1. The rotor has an unbalance, the radius of unbalance being e_u. The unbalance creates a rotating force of magnitude equal to the centrifugal force due to the unbalanced mass.

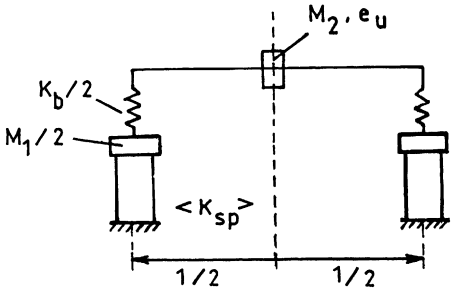

Fig. 7. The rotor–shaft system.

2.3.2. Equations of motion

Following Ref. [2] the equations of motion are written below:

$$M_2\ddot{x}_2 + c_i\dot{x}_s + K_s x_s + c_i\omega y_s = M_2 e_u \omega^2 \cos\omega t, \tag{26}$$

$$K_b x_{jo} - c_i\dot{x}_s - K_s x_s - \omega c_i y_s = 0, \tag{27}$$

$$M_1\ddot{x}_1 + 2K_1^c K(\,)x_1 + 2K_2^c K(\,)y_1 - K_b x_{jo} = 0, \tag{28}$$

$$M_2\ddot{y}_2 + c_i\dot{y}_s + K_s y_s - c_i\omega x_s = M_2 e_u \omega^2 \sin\omega t, \tag{29}$$

$$K_b y_{jo} - c_i\dot{y}_s - K_s y_s + \omega c_i x_s = 0, \tag{30}$$

$$M_1\ddot{y}_1 + 2K_2^c K(\,)x_1 + 2K_3^c K(\,)y_1 - K_b y_{jo} = 0, \tag{31}$$

where "x_m" and "y_m" are the generic displacements for $m = 1, 2, jo, s$ where the suffixes "1" and "2" stand for the absolute displacement of the bearing mass and rotor mass, respectively, suffix "*jo*" denotes the net deformation of the bearing element and the suffix "*s*" denotes the displacement of rotor mass with respect to the ends, i.e., $x_s = x_2 - x_j - x_1$ and $y_s = y_2 - y_j - y_1$.

2.3.3. Response calculation

Synchronous steady state response has been found out in this section. Substituting in the equations from (25) to (30) $x_m = X_m e^{i\omega t}$ and $y_m = Y_m e^{i\omega t}$, for $m = 1, 2, jo$, where $i = \sqrt{-1}$, X_m and Y_m are complex numbers, using the *non-dimensional terms*

$$\alpha = M_1/M_2, \quad \beta_b = K_b/K_s, \quad \beta_1 = K_1/K_s, \quad \beta_2 = K_2/K_s, \quad \xi_1 = C_1/c_c, \quad c_c = 2M_2\omega_n,$$

$$\delta = \frac{\omega}{\omega_n}, \quad \omega_n = \sqrt{\frac{K_s}{M_2}}, \quad \beta_{sp1} = \frac{K_1^c K_{real}}{K_s}, \quad \beta_{sp2} = \frac{K_2^c K_{real}}{K_s}, \quad \beta_{sp3} = \frac{K_3^c K_{real}}{K_s},$$

$$\frac{K_{real}}{K_s} = \left\{\frac{\beta_1\beta_2^2 + 4(\beta_1+\beta_2)\xi_1^2\delta^2}{\beta_2^2 + 4\xi_1^2\delta^2}\right\}, \quad \eta = \frac{2\beta_2^2\xi_1\delta}{\{\beta_1\beta_2^2 + 4(\beta_1+\beta_2)\xi_1^2\delta^2\}}$$

and solving the resulting simultaneous equations X_m and Y_m can be found out.

$$x_m = real(X_m e^{i\omega t}), \quad y_m = imaginary(Y_m e^{i\omega t}). \tag{32}$$

The vector form of displacement can be obtained by writing the displacements in the form of

$$z_m = x_m + iy_m. \tag{33}$$

Non-dimensional unbalanced response amplitude is found out by dividing $|z_m|$ for $m = 1, 2, jo$ by e_u. Non-dimensional steady state response amplitude of the rotor is given by the expression

$$UBR = \max(|z_2|)/e_u. \tag{34}$$

2.3.4. Special case of no cross-coupling

If corresponding to any arrangement of the sectors the value of $K_2^c = 0$ and $K_1^c = K_3^c = K_{sp}$ then, for that arrangement of the polymeric sectors, forces in the X and Y directions will be uncoupled. For such cases Eqs. (25)–(30) can be assembled and reduced to only 3 equations by putting $z_m = x_m + \mathrm{i}y_m$ and written below for $m = 1, 2, jo$. The equations can be found in Ref. [14]:

$$M_2\ddot{z}_2 + c_i\dot{z}_s + (K_s - \mathrm{i}\omega c_i)z_s = M_2 e_u \omega^2 \mathrm{e}^{\mathrm{i}\omega t}, \tag{35}$$

$$K_b z_{jo} - c_i z_s - (K_s - \mathrm{i}\omega c_i)z_s = 0, \tag{36}$$

$$M_1\ddot{z}_1 + 2\langle K_{sp}\rangle z_1 - K_b z_{jo} = 0. \tag{37}$$

In Eq. (36), $\langle K_{sp} \rangle$ is the support stiffness operator and is equal to $K_{\mathrm{sup}}K(\,)\,K_{\mathrm{sup}}$ is a factor consisting of the geometrical parameters of the sectors.

Following the above solution process, putting $\beta_{sp1} = \beta_{sp3} = \beta_{sp}$, $\beta_{sp2} = 0$ and using the other non-dimensional terms Eqs. (34)–(36) can be reduced to the following form:

$$\begin{bmatrix} (1-\delta^2) & -1 & -1 \\ 1 & -(1+\beta_b) & -1 \\ 0 & \beta_b & \{\alpha\delta^2 - 2\beta_{sp}(1+\mathrm{i}\eta)\} \end{bmatrix} \begin{Bmatrix} Z_2 \\ Z_{jo} \\ Z_1 \end{Bmatrix} = \begin{Bmatrix} e_u\delta^2 \\ 0 \\ 0 \end{Bmatrix}. \tag{38}$$

From Eq. (37) non-dimensional unbalance response amplitude Z_m/e_u can be found out for $m = 1, 2, jo$ and given below:

$$\frac{Z_2}{e_u} = \frac{[-\{\alpha\delta^2 - 2\beta_{sp}(1+\mathrm{i}\eta)\}(1+\beta_b) + \beta_b]\delta^2}{\{\alpha\delta^2 - 2\beta_{sp}(1+\mathrm{i}\eta)\}\{\delta^2(1+\beta_b) - \beta_b\} - \beta_b\delta^2}, \tag{39}$$

$$\frac{Z_{jo}}{e_u} = \frac{[\alpha\delta^2 - 2\beta_{sp}(1+\mathrm{i}\eta)]\delta^2}{\{\alpha\delta^2 - 2\beta_{sp}(1+\mathrm{i}\eta)\}\{\delta^2(1+\beta_b) - \beta_b\} - \beta_b\delta^2}, \tag{40}$$

$$\frac{Z_1}{e_u} = \frac{\beta_b\delta^2}{\{\alpha\delta^2 - 2\beta_{sp}(1+\mathrm{i}\eta)\}\{\delta^2(1+\beta_b) - \beta_b\} - \beta_b\delta^2}. \tag{41}$$

Non-dimensional unbalanced response amplitude of the rotor is

$$UBR = |Z_2|/e_u. \tag{42}$$

The undamped natural frequencies can be found out from Eq. (38) by putting $\eta = 0$ and equating the determinant of the system matrix to 0. The system in this case has two degrees of freedom and has two natural frequencies denoted by two non-dimensional quantities δ_1 and δ_2 which change with the frequency of excitation.

2.4. Stability limit speed

The SLS or the stability threshold of the system can be calculated by using Routh's criterion as was done by Dutt and Nakra [8]. Detailed process has not been given here for making this paper brief. Substituting $z_2 = Z_2 e^{i\lambda t}$, $z_j = Z_j e^{i\lambda t}$, $z_1 = Z_1 e^{i\lambda t}$ in the equations of motion for free vibration and putting $R = \lambda/\sqrt{K_s/M_2}$ the characteristic equation can be written.

3. Results and discussion

In the support system comprising of sectors the material of each has been considered same. Presented under this section are the results and discussions concerning three topics, (1) support characteristics for different placement of sectors, (2) unbalanced response amplitude and effect of supports and (3) parametric analysis to obtain optimum parameters for support sectors. Non-dimensional parametric values of the system studied are chosen as $\alpha = 0.4$, $\beta_b = 2.0$, $\beta_1 = 0.01$, $\beta_2 = 0.5$, $\xi_1 = 0.1$, $\mu = 0.5$, $\mu_p = 0.5$.

3.1. Support characteristics

From the expression of K_{real} and η, it may be seen that these quantities change with the frequency of excitation. Whereas K_{real} monotonically increases with the excitation frequency, η may increase or decrease. The property of the support system with polymer sectors is also in general frequency dependent. It will be interesting to see the frequency-dependent characteristics of a few support systems to start with. The sectors are called symmetrically placed, when all the sectors are of same length, i.e., each sector subtends same angle at the bearing centre and are equidistant along the circumference, otherwise the placement is non-symmetrical. Figs. 8(a) and (b) show the sector arc length (in terms of angle subtended by a sector at the bearing centre) placement and the corresponding characteristics of the support system comprising four non-symmetrically placed sectors respectively. Fig. 8(b) shows that β_{sp2}, the non-dimensional cross-coupled stiffness is negative. Therefore, there may exist the possibility of instability. Fig. 9(a) shows a support system consisting of four symmetrically placed sectors each subtending an angle of 18° at the bearing centre. Corresponding characteristics in Fig. 9(b) show no cross-coupling. Moreover the stiffness in X and Y directions are same. Similar effect is noticed from Figs. 10(a) and (b), where eight symmetrically placed sectors (each subtending 10° at the bearing centre) were chosen. It may be concluded that sectors having arbitrary length and placed arbitrarily that is without any visible symmetry, give rise to cross coupled stiffness which may be unwanted when they become negative. Forces in X and Y co-ordinates are not coupled if sectors are of same length and placed symmetrically. In the subsequent studies, therefore, sectors of equal arc length, i.e., sectors subtending equal angle at the bearing centre have been considered.

3.2. Unbalanced response amplitude and effect of supports

Unbalanced response has been studied and reported here to visualize the mechanism of obtaining the optimum dimension of the polymeric supports for providing *optimum damping* at

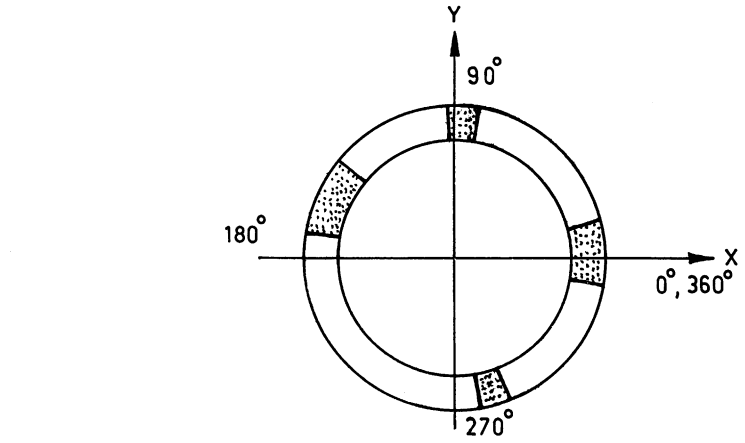

(a)

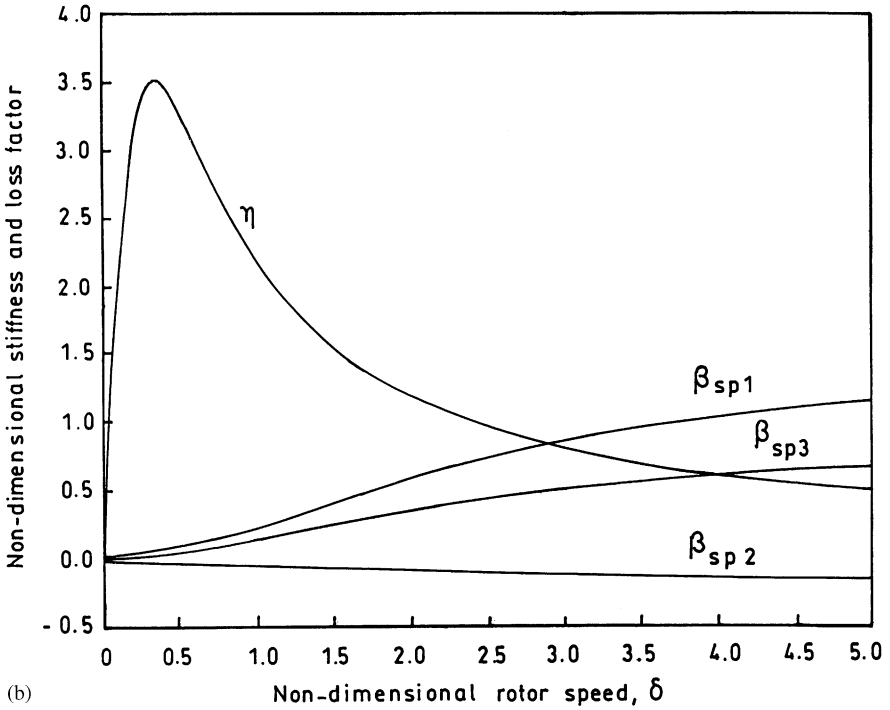

(b)

Fig. 8. (a) Support system with four unsymmetric sectors and (b) the characteristics.

the supports and achieving *global minimum of the unbalanced rotor response amplitude* for any particular support material.

In this study 4 sectors, each subtending same angle at the bearing centre, have been considered to be placed 90° apart and symmetrically with respect to the X and Y axes. The arrangement is

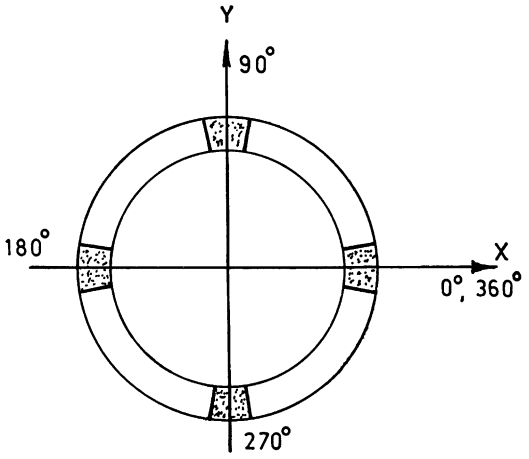

(a)

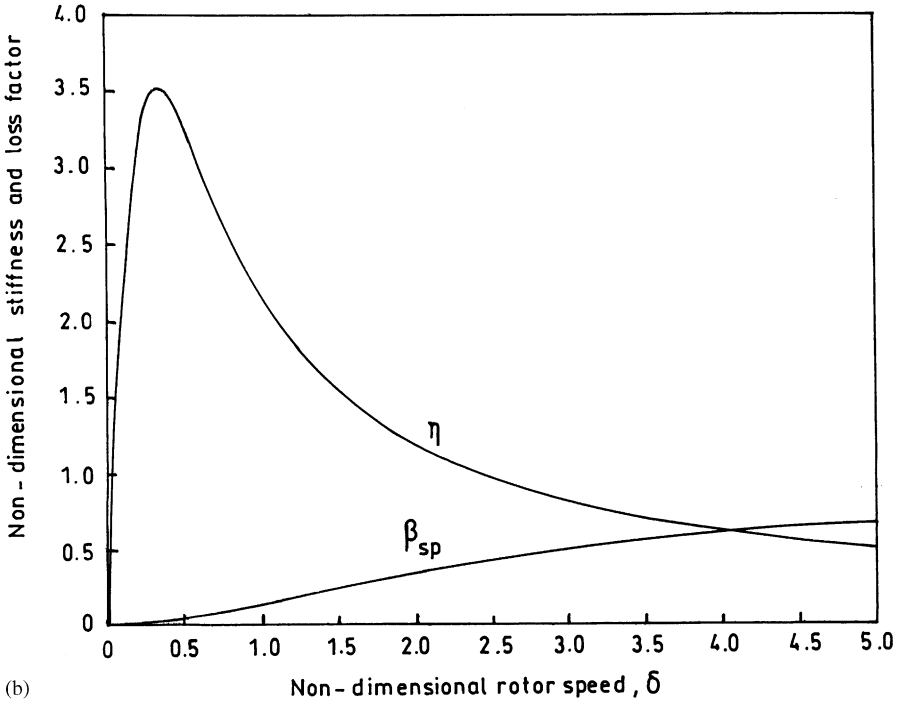

(b)

Fig. 9. (a) Support system with four symmetric sectors and (b) the characteristics.

shown in Fig. 9(a). The angles subtended by each sector at the bearing centre have been selected as 8°, 12°, 18°, 40° in the Figs. 11–14, respectively. Figs. 11(a)–14(a) show the plot of UBR, δ_1 and δ_2 with varying non-dimensional rotational frequency δ. Figs. 11(b)–14(b) show the real part vs. imaginary part of the non-dimensional rotor response Z_2/e_u. These plots are also called Nyquist

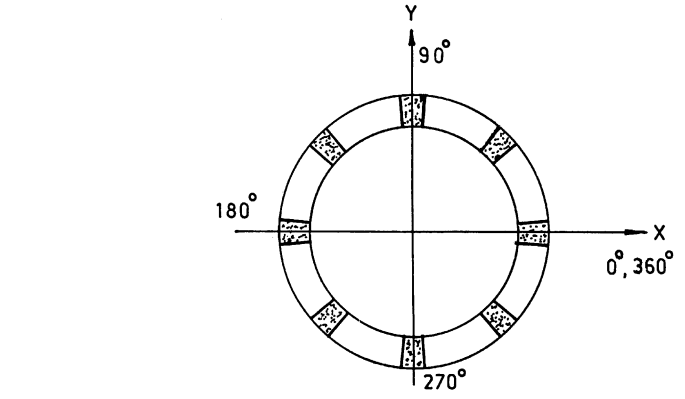

Support characteristics for the support system with 8 sectors from -5°- +5°, 40°- 50°, 85°- 95°, 130°- 140°, 175°-185°, 220°- 230°, 265°-275°, 310°- 320°

(a)

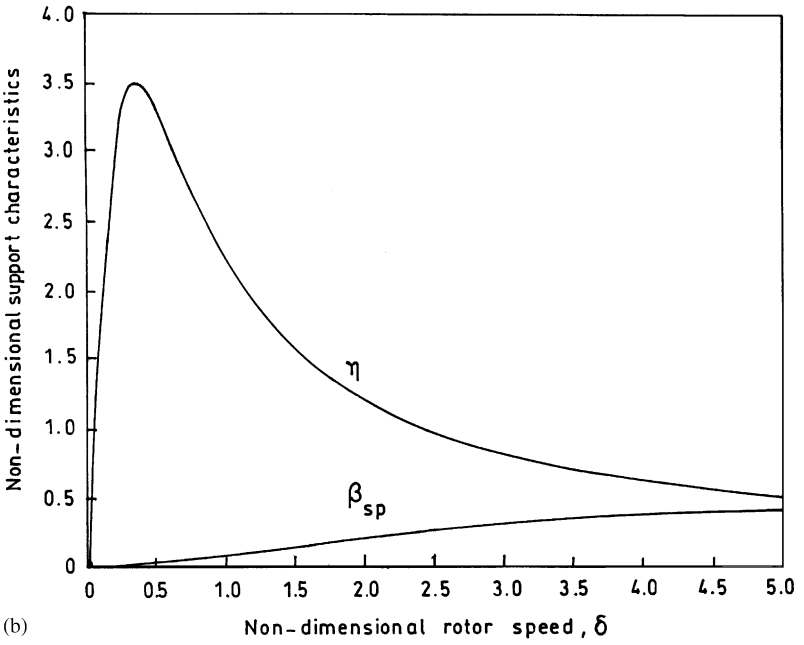

(b)

Fig. 10. (a) Support system with eight symmetric sectors and (b) the characteristics.

plots [15]. Figs. 11(a) to 14(a) show that δ_1 and δ_2 monotonically increase with δ. This happens because stiffness of the polymeric sectors increase with increasing frequency of excitation. Whenever any natural frequency of the system is intercepted by the sweeping frequency of excitation, resonance occurs and the corresponding peaks are expected to occur in the close vicinity of the point of interception. The points of interception are shown in the figures as the points of intersection of the 45° line with the plots of δ_1 and δ_2. In Figs. 11(a) and 12(a) each, two

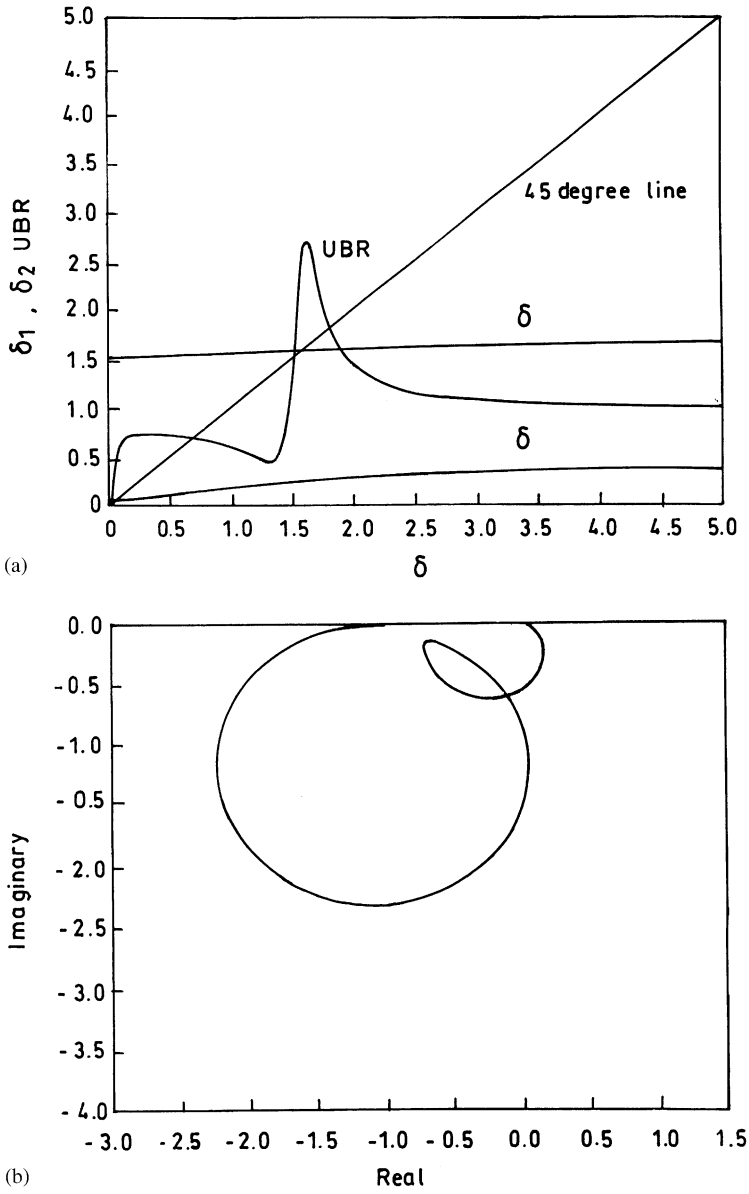

Fig. 11. (a) Rotor response with 8° sectors and (b) real versus imaginary plot for 8° sectors.

peaks (corresponding to two degrees of freedom), occur in the close vicinity of the corresponding point of intersection but in Figs. 13(a) and 14(a) each, only one peak shows up instead of two. In Fig. 14(a) the only peak is not in the neighborhood of either point of intersection. This can also be verified by looking at Figs. 11(b)–14(b). Whereas in Fig. 11(b), the plot completes two loops, signifying the existence of two peaks, in the latter ones, encirclement in the middle has been reduced to kinks, a deep kink in Fig. 12(b) and light kinks each in Figs. 13(b) and 14(b),

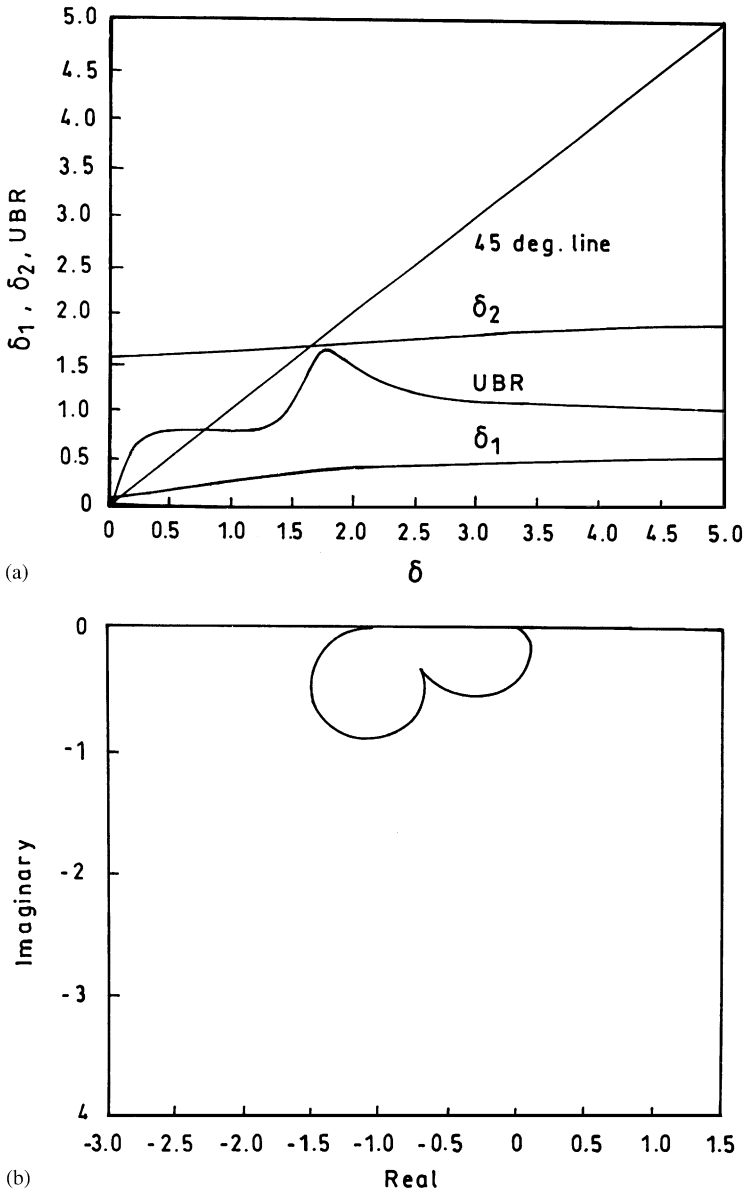

Fig. 12. (a) Rotor response with 12° sectors and (b) real versus imaginary plot for 12° sectors.

respectively. These plots differ from the nature of the Nyquist's plot given in Ref. [15], for any two-degree-of-freedom system with constant stiffness, in the sense that, both the loops are not *physically* complete. This is principally due to *the dependence of stiffness and loss factor on the frequency of excitation.* Thinking heuristically, the reduction in the number of encirclement by one, is, as if, equivalent to losing one degree of freedom. This behavior is primarily due to the effect of high damping, which masks one of the peaks. Steady global reduction of UBR is observed as the angle is increased from 8–18° degrees but further increment of the angle proves

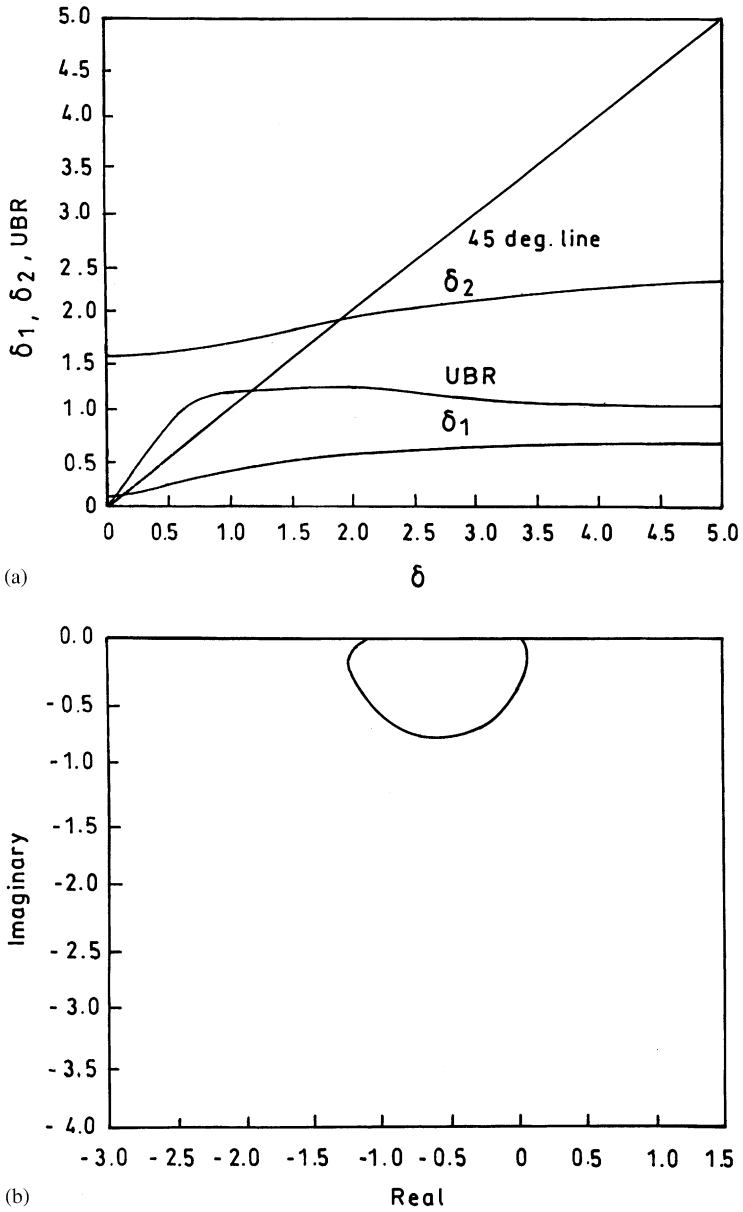

Fig. 13. (a) Rotor response with 18° sectors and (b) real versus imaginary plot for 18° sectors.

deleterious. Therefore with the present parametric values of the system, a length of the sector subtending 18° at the bearing centre is optimum. Different optimum values are obtained with different set of parametric values.

Examination of the figures may infer that the arc length of the sector should be increased up to the point when the real versus imaginary plot (Nyquist Plot) of the rotor response apparently ceases to show as many encirclements as the degrees of freedom. This is an important observation and may also serve as a quick useful indicator to reaching optimality.

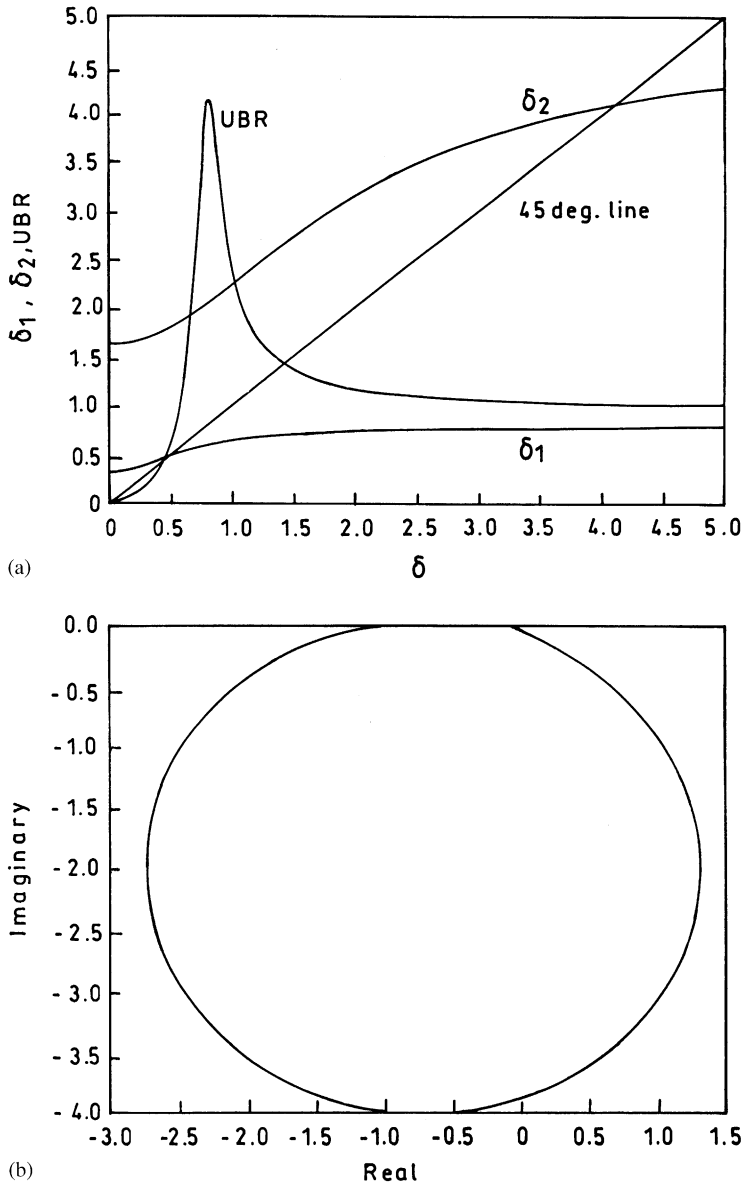

Fig. 14. (a) Rotor response with 40° sectors and (b) real versus imaginary plot for 40° sectors.

Optimum values of other support parameters have been found out using parametric analysis reported in the next section.

3.3. Parametric analysis

Parametric analysis of the UBR has been done to find out optimum geometric parameters of the sectors (angle θ subtended by a sector and thickness ratio μ_p) and to assess the effect of other support parameters ($\alpha, \beta_1, \beta_2, \xi_1$). For this analysis the value of one parameter, chosen at a time,

has been varied with the values of others kept constant at the respective chosen values. Chosen constant values for the system under study are given above under Section 3.1. In each of the figures from 15–19 the "global peak unbalanced frequency response amplitude of the rotor" (GPUBR) has been plotted with varying value of the chosen parameter.

Fig. 15 shows the variation of GPUBR with the angle subtended by each sector. This shows that the minimum response amplitude is achieved with $\theta = 18^{\circ}$ for the chosen set of parameters of the system. The *mechanism of obtaining* the optimum value was shown in Figs. 11–14. Therefore polymeric material sectors of optimum arc length, rather than a full annular length, are more useful for reducing global peak rotor response amplitude.

Fig. 16 shows the variation of the GPUBR with the non-dimensional thickness parameter μ_p. It is observed that μ_p has an optimum value of 0.48 corresponding minimum rotor response. So the often-apparent idea that "the thicker the polymeric layer the minimum becomes the response" is not true. There exists an optimum thickness of the layer depending upon the parametric values of the system. The same value could be obtained by following the Nyquist plot drawn in Section 3.2.

Fig. 17 shows the variation of GPUBR with support mass ratio α. It is seen that there exists an optimum value of α corresponding to minimum response amplitude.

Fig. 18 shows the variation of GPUBR with varying values of β_1 and β_2, the primary and secondary support stiffness ratios respectively. Like before it may be found that there exist optimum values of the parameters corresponding to minimum response amplitude. Considering the 3-element model given in Fig. 1(b) it may be noticed that the ease of deflection of the support and the accompanying dissipation of vibratory energy depends upon the magnitude of K_1 or the value of β_1 in non-dimensional form. Very high value of β_1 results in low deformation of the support and hence GPUBR increases. Examination of Eqs. (24) and (25) shows that the value of damping force offered by the 3-element model is obtained by multiplying the expressions of K_{real}

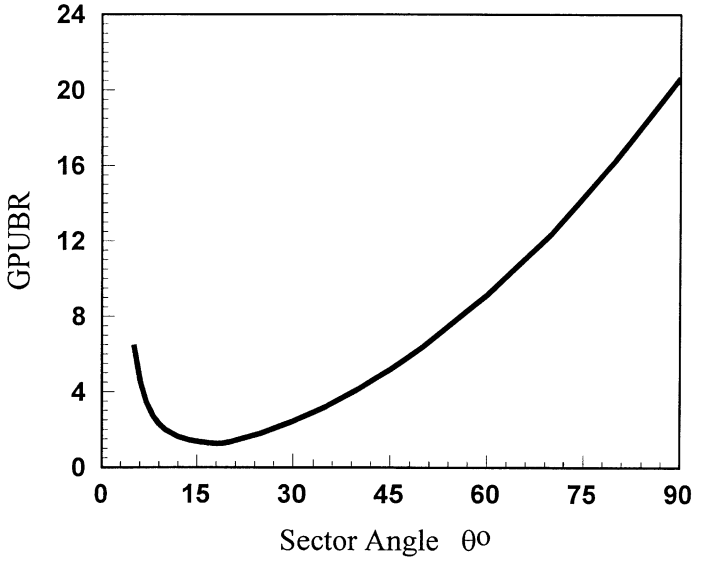

Fig. 15. Variation of global peak unbalanced response amplitude with angle subtended by a sector.

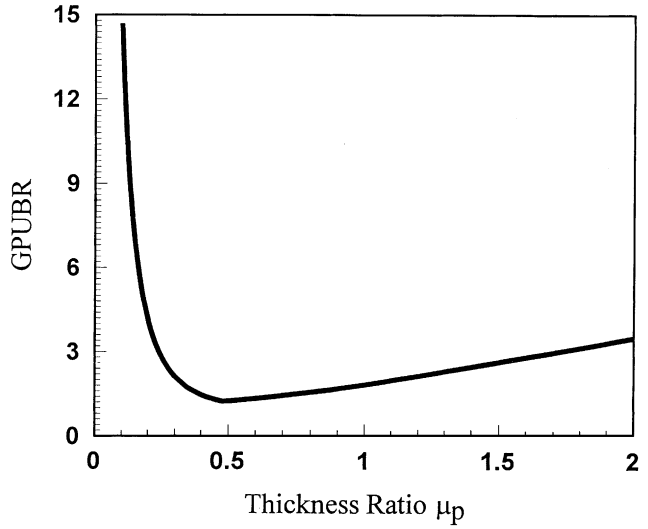

Fig. 16. Variation of global peak unbalanced response amplitude with the thickness of the sector.

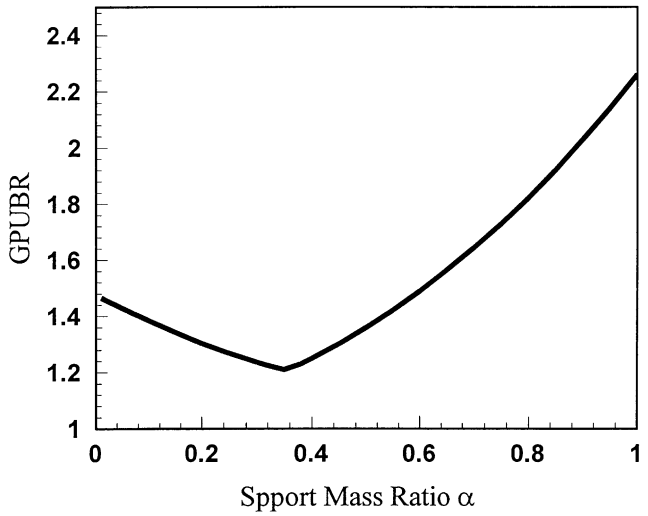

Fig. 17. Variation of global peak unbalanced response amplitude with the thickness of the support mass ratio.

and η given by Eq. (25). Contrary to the apparent feeling, it may be noticed that the damping force increases as K_2 (or β_2 in non-dimensional form) increases and C_1 (or ξ_1 in non-dimensional form) decreases. This happens because the support stiffness and damping elements K_2 and C_1 are connected in series. A high damping polymer, very much suitable for containing vibration level, can, therefore, be obtained with high values of K_2 for the 3-element model. Fig. 18 shows that any value of $\beta_2 > 0.4$ is approximately suitable but $\beta_2 = 0.5$ corresponds to minimum response amplitude.

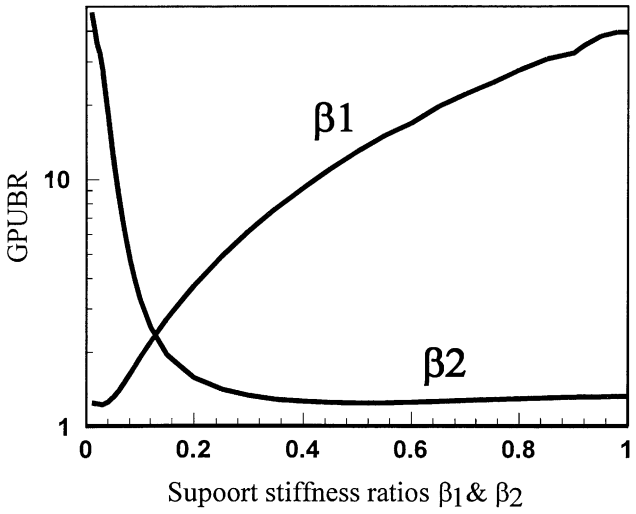

Fig. 18. Variation of global peak unbalanced response amplitude with primary and secondary support stiffness ratios.

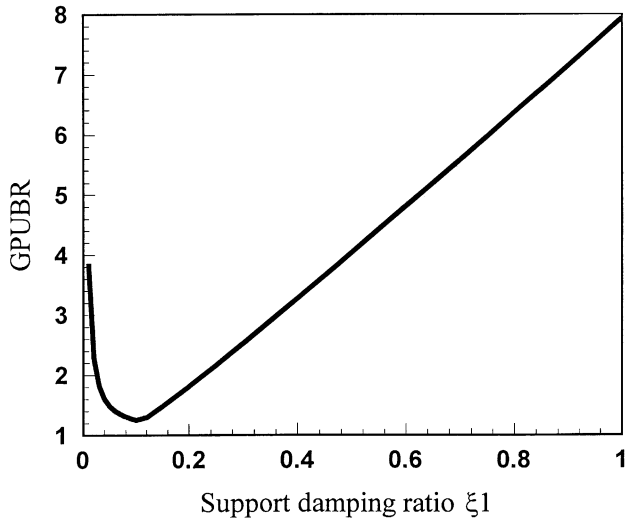

Fig. 19. Variation of global peak unbalanced response amplitude with support damping ratio.

Fig. 19 shows the variation of GPUBR for varying values of ξ_1. It is noticed that there exists an optimum value of $\xi_1 = 0.1$ for minimum value of GPUBR. As the value of ξ_1 increases beyond the optimum, the support approaches towards a rigid one, lending it more difficult to be deformed and failing to dissipate the energy of vibration more and more as a result.

Fig. 20 shows the non-dimensional SLS of the rotor–shaft system for different arc length of the sectors and different thickness ratios. It may be seen that any combination of arc length and the

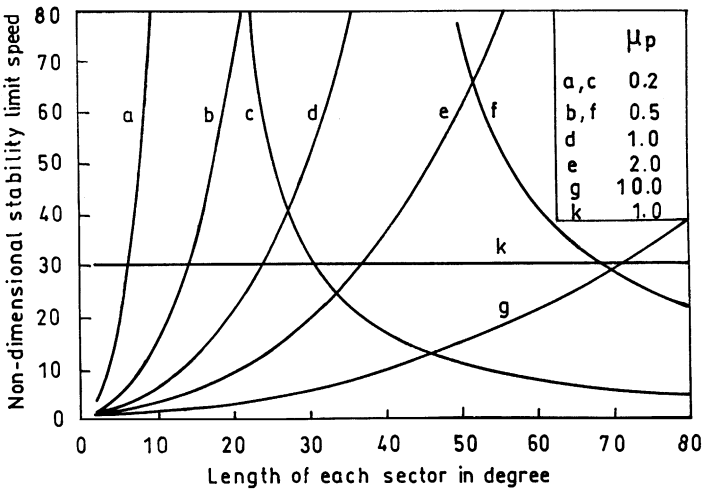

Fig. 20. Non-dimensional SLS for different length of sectors.

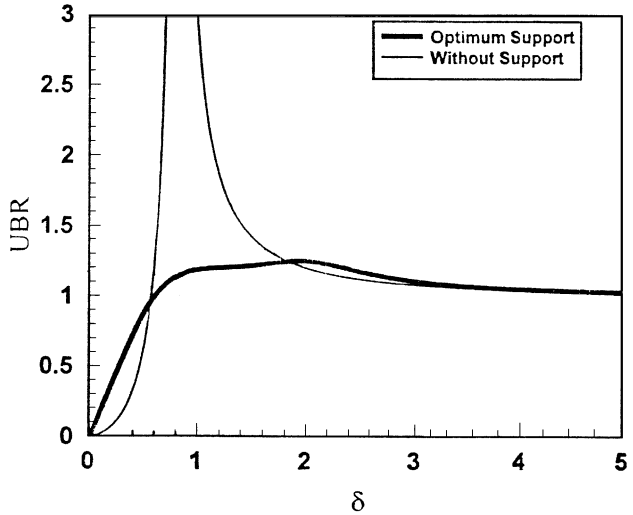

Fig. 21. Comparison of unbalanced response amplitude between rotor–shaft system with and without supports.

thickness of the sector do not give high SLS. Moreover it may be noticed that there exists optimum value of the arc length for which the SLS is very broad. For the system parameters chosen in this paper four symmetric sectors placed 90° apart and each having $\theta = 18°$ and $\mu_p = 0.5$ will give a very high SLS. The graph marked with "$k = 1$" shows the one obtained by considering the multiplying factor $K_{\text{sup}} = 1$ corresponding to the case when the geometrical effects are not considered. The SLS is constant. It may be noticed that, for a particular material, very low UBR and very high SLS are possible to get with proper dimensional design of the polymeric sectors.

3.4. Comparison

UBR has been plotted in Fig. 21 for two cases:

(1) where the rotor–shaft is mounted on only bearings at the ends (marked as "Without supports") and

(2) where the same system is mounted on bearings at the ends supported on optimum polymeric support system comprising of four symmetrically placed sectors, $\theta = 18$ degree and $\mu_p = 0.5$ for each. The same non-dimensional system parameters given above have been used. This clearly shows that the optimum supports give much less *UBR* and are therefore superior to the situation of having no supports.

4. Conclusions

1. Polymeric sectors, not full annular polymeric inserts serve as very efficient rotor supports.

2. High value of K_2 in the 3-element model signifies polymers with high damping capacity, very much useful for vibration control.

4. Symmetrically placed sectors rather than unequal and non-symmetrically placed ones are useful as the latter give rise to cross-coupled stiffness, which, if negative, can give rise to the problem of instability.

5. For the set of parameters taken in this problem, a support system consisting of 4 sectors placed 90° apart, each subtending an angle of 18° at the bearing centre and having thickness approximately $\frac{1}{2}$ of the bearing outer race give minimum unbalanced response amplitude. The same sectors will give quite high SLS. Here the angle θ may be varied by -2° and μ_p by -0.04 for approximately obtaining the minimum unbalanced response and maximum SLS.

6. In this work polymeric supports were chosen but other than polymeric supports capable of generating same characteristics will also reduce the vibration response equally.

Acknowledgements

I do hereby gratefully acknowledge the kind help given by the Japan Society for the Promotion of Science (JSPS) for completing this work. I am grateful to Prof. N. Okubo for his kind guidance at all the stages of this work. I express my thanks and gratitude to Mr. N. Chiba for his kind help in knowing many things, which are very important.

References

[1] J.W. Lund, The stability of an elastic rotor in journal bearing with flexible damped supports, Journal of Applied Mechanics, Transactions of the American Society of Mechanical Engineers 32 (4) (1965) 911–920.

[2] R.G. Kirk, E.J. Gunter, The effect of support flexibility and damping on the synchronous response of a single mass flexible rotor, Journal of Engineering for Industry, Transactions of the American Society of Mechanical Engineers 94 (1) (1972) 221–232.

[3] W.D. Pilkey, et al., Efficient optimal design of suspension system for rotating shafts, Journal of Applied Mechanics Transactions of the American Society of Mechanical Engineers 98 (3) (1976) 1026–1029.
[4] A.K. Mallik, Principles of Vibration Control, Affiliated East West Press, New Delhi, 1990, pp. 70–92.
[5] M. Darlow, E. Zorzi, Mechanical Design Handbook for Elastomers, CR 3423 NASA, 1981.
[6] E. Zorzi, et al., Elastomer damper performance—a comparative study with squeeze film damper for supercritical power transmission shaft, ASME Gas Turbine Conference, March 1980.
[7] R.D. Corsaro, L.H. Sperling, Sound and Vibration Damping with Polymers, American Chemical Society, Washington, DC, 1990.
[8] J.K. Dutt, B.C. Nakra, Stability of rotor systems with viscoelastic supports, Journal of Sound and Vibration 153 (1) (1992) 89–96.
[9] J.K. Dutt, B.C. Nakra, Vibration response reduction of a rotor shaft system using viscoelastic polymeric supports, Journal of Vibration and Acoustics, Transactions of the American Society of Mechanical Engineers 115 (1993) 221–223.
[10] K.C. Panda, J.K. Dutt, Design of optimum support parameters for minimum rotor response and maximum stability limit, Journal of Sound and Vibration 223 (1) (1999) 1–21,.
[11] J.K. Dutt, Studies on Dynamics of Rotating Systems on Viscoelastically Damped Supports, Ph.D.Dissertation, IIT Delhi, 1993.
[12] D.R. Bland, Linear Viscoelasticity, Pergamon Press, Oxford, 1960.
[13] K. Bhattacharyya, J.K. Dutt, Unbalance response and stability analysis of horizontal rotor system mounted on nonlinear rolling element bearings with viscoelastic supports, Journal of Vibration and Acoustics, Transactions of the American Society of Mechanical Engineers 119 (1997) 539–544.
[14] J.K. Dutt, T. Toi, N. Chiba, Rotor vibration reduction using polymeric supports, Proceedings of ISMA 25 Conference, Vol. 1, 13–15th September 2000, Katholieke Universeteit, Leuven, Belgium, 2000, pp. 69–75.
[15] D.J. Ewins, Modal Testing Theory and Practice, Research Studies Press, 1984.